04

Collisionless scenario of multi-component cathode plasma expansion in vacuum diode

© V.Y. Kozhevnikov, A.V. Kozyrev, A.O. Kokovin

Institute of High Current Electronics, Siberian Branch, Russian Academy of Sciences,
634055 Tomsk, Russia
e-mail: kozyrev@to.hcei.tsc.ru

Received July 15, 2025
Revised September 30, 2025
Accepted October 6, 2025

Based on the fundamental physical kinetics of plasma, the concept of a collisionless scenario of expansion of a multi-component cathode plasma in a vacuum gap to which an external voltage is applied is demonstrated. It is shown that the pulse-periodic mode of plasma emission does not change the previously identified electrodynamics of the current-carrying plasma expansion, but generates a non-stationary profile of the electric potential in the gap in the form of a so-called „potential hump". Within the framework of the basic scenario, it is shown that the calculated plasma expansion speeds are in good agreement with the experimentally observed data, and for ions of different charge multiplicities. Calculation of the electron beam kinetics showed that the current density in a planar vacuum diode with a plasma cathode is several times higher than the estimate of the Child–Langmuir current density. The application of kinetic theory allows us to reveal the fundamental properties of the ECtonic mechanism of explosive electron emission both in the general process of plasma expansion and in the self-consistent dynamics of the distribution functions of electrons, singly and doubly charged ions

Keywords: vacuum discharge, physical kinetics of plasma, plasma cathode, ions in a vacuum arc.

DOI: 10.61011/TP.2026.02.62877.183-25

Introduction

A vacuum high-current discharge phenomenon widely used in the modern electrical engineering and high-power electronics is a complex physical process, which is studied in a set of fundamental monographs [1–4]. Deep understanding of vacuum discharge is critical for improving physical characteristics of a wide range of instruments and devices such as vacuum transmission and forming lines, electron and ion sources and accelerators, high-current electron beam microwave generators and compact X-ray pulse generators [1].

Vacuum discharge is a complex process including three successive stages — vacuum breakdown [2], vacuum spark [3] and vacuum arc [4]. Modern study of vacuum breakdown is indissolubly related to an explosive electron emission phenomenon [2,3]. Explosive emission is a brief synonym of a complex process where a compact nonsteady plasma formation, emission center or ecton being a source of cathode substance electrons and ions, is generated on a vacuum diode cathode. This study doesn't address causes and details of explosive emission, but is focused on the next vacuum discharge stage — expansion of the explosive emission center cathode plasma in a vacuum diode, to which high voltage is applied from an external source.

This vacuum breakdown transition (from breakdown initiation to high-current arc) phase, vacuum spark phase, defines one of the key discharge parameters — arc formation time, i.e. high-current discharge stage delay time after discharge initiation. This time is determined by the rate of vacuum diode filling with dense plasma. At this stage (hereinafter referred to as the vacuum switching stage), principal current in a diode is carried by electrons emitted from the ecton plasma boundary and accelerated by a difference of potentials applied to the gap. Anode ion fluxes are also generated at this stage. This phenomenon was first discovered and experimentally investigated by Plyutto et al [5–7]. At the vacuum switching stage, typical plasma expansion velocities exceed 10^6 cm/s, and ions transfer up to 12% of the total charge on a collector (anode) [8]. Kinetic energy of ions passed through the anode is usually from tens to hundreds of electron-volts [9]. This effect was reliably experimentally verified and described in a large body of literature on vacuum discharge, for example, in [2,5,9].

Physical mechanism behind ion acceleration in an „anomalous" for them direction (positively charged ion travel to the positive electrode) has been a subject of discussion in various academic schools and research groups for decades now [5,9–11]. The main discussion is between two concepts capable of explaining the anomalous direction and high velocity of ions passed through the anode. The first hypothesis was proposed in a pioneer work [5], where an assumption was put forward that there was an „electric potential hump" in the explosive emission center area. A local maximum of electric potential provided, according to the authors of [5–7], both the direction and observed

velocity of ions. But the presence of this local potential hump hasn't been confirmed yet by any experimental measurements.

The second hypothesis for the fast ion and plasma acceleration mechanism treats this process similar to the way in which gas flowing from a narrow nozzle is accelerated up to supersonic speeds. Attempts to describe plasma motion theoretically in the framework of fluid (hydrodynamic) models didn't suggest non-monotonic distribution of potential [10], and internal electron-ion friction force was taken as the main force accelerating ions in the „anomalous" direction. This mechanism was called the „electron wind acceleration". On the assumption of extremely high plasma densities in the emission center, which justify utilization of hydrodynamic approximation for plasma description, theory of multi-fluid vacuum discharge plasma jet [10], which provides equal velocities of ions with different charge number in anode flux, was built. Unfortunately, there is no agreement among experimenters regarding this question: there is solid evidence suggesting both different [5,9,12] and similar velocities [8,10,13] of ions with different charge number in anode-directed flux. In addition, describing plasma in hydrodynamic approximation as a continuous medium is not quite adequate to vacuum discharge conditions high density gradient of particles.

A significant progress in the discussion has been achieved owing to modern physical kinetics methods, which constitute, in the authors' opinion, the most adequate approach to describing plasma motion in vacuum discharge. Kinetic approach allowed developing simple models of cathode plasma expansion in planar [14–16] and geometrically inhomogeneous [17,18] vacuum gaps. Calculations has shown that the main cause of fast cathode plasma expansion and anomalous ion acceleration is an electrodynamic mechanism based on initiation of a localized region of non-monotonic potential distribution representing a transient virtual cathode. Kinetic approach clarified the general cause of anode ion acceleration and allowed calculation of average cathode plasma expansion velocities. Analysis of solutions of kinetic equations has shown that elastic collisions of charged particles during plasma motion play a minor role and plasma may be described within collisionless approximation. Kinetic theory of collisionless multicomponent plasma expansion has detected inadequacy of the initial „potential hump"hypothesis, but has demonstrated a new ion acceleration mechanism in a „virtual cathode" structure [14,16,17].

All these conclusions were based on a substantial assumption: these calculations assumed cathode plasma emission to be continuous in time, while experiments show that electron current in the ecton flows with discrete spikes [2,3]. Explosive plasma emission is initiated, exists during a certain period of time and ends. Then this process is resumed repeatedly. Pulse-periodic dense plasma emission on cathode modulates the electron current on anode and ion current in cathode plasma causing potential redistribution in the gap [18]. It is the pulse-periodic mode of cathode plasma generation in the gap where the „potential hump" profile is implemented. This unobvious result allows us to propose a new vacuum spark stage scenario for discussion by academic community: high-voltage stage of collisionless current-carrying plasma expansion initiated on cathode in pulse-periodic mode.

This study investigates the effect of pulse-periodic cathode plasma emission mode on collisionless plasma expansion and electron and ion flux generation Physical kinetics method investigates the three-component plasma expansion process and spatiotemporal potential dynamics, electron and ion distribution functions over pulses within the full emission current variation cycle. Owing to utmost physical simplicity of the kinetic model (one-dimensional geometry, absence of particle collisions, predefined plasma composition, controlled voltage applied to the diode), this scenario can be treated as a basic one related to all vacuum discharges. The computational model shown below and kinetic calculation results demonstrate all common patterns of filling the vacuum gap with plasma and subsequent transfer of charge particles in these conditions.

1. Kinetic model of current-carrying plasma expansion in a vacuum diode

Consider a vacuum diode in the form of a planar one-dimensional region formed by plane-parallel electrodes — cathode and anode. The choice of plane problem is conditioned by simplicity of analysis and by the fact that it is characterized by a single spatial parameter — gap length. It is not a matter of principle, for example, a similar one-dimensional axisymmetric problem is solved in [16].

The distance between electrodes is denoted by D, and the diode cross-section area is denoted by S (this parameter has no fundamental impact on the physical solution of problem, but is necessary to calculate full discharge current). Distribution functions characterizing physical state of electron and ion ensembles will depend solely on the x coordinate, longitudinal momentum component p_x and time t. Key point of the model is is a boundary condition at cathode. We suppose that quasi neutral multi-component plasma emission from the cathode surface (at $x = 0$) starts at time $t = 0$ and is characterized by the pre-defined dependence of number density on time $n(t)$. It is hereinafter assumed for clarity that the cathode emission plasma has three-component composition, includes electrons, singly-charged and doubly-charged ions. Such plasma composition is not abstract, but is typical of cathodes made of such materials as magnesium, zinc, germanium, strontium, indium, etc. [19]. For the purpose of this study, calculations use data for zinc (Zn, $m_i = 65.38$ amu), in which, according to the experimental data, singly-charged ions Zn^+ constitute [19],

80 % of the total fraction of ions, and the remaining portion consists of doubly-charged ions Zn^{++}.

This study adheres to a previously developed general method of using physical kinetics of vacuum breakdown [14]. Cathode plasma components are unambiguously described by corresponding single-particle distribution functions, which obey the collisionless Vlasov equations. Vacuum diode is explored without external magnetic field, and the magnetic field of discharge current is also neglected, which limits the model applicability by not very high currents (up to 100 A). Self-consistent description of electromagnetic interaction of particles is limited to the mutual influence between particles through electrostatic forces, which is considered by inclusion of the Poisson equation into the system of equations of the mathematical model:

$$\frac{\partial f_e}{\partial t} + \frac{p_x}{m_e}\frac{\partial f_e}{\partial x} - qE_x\frac{\partial f_e}{\partial p_x} = 0,$$

$$\frac{\partial f_+}{\partial t} + \frac{p_x}{m_i}\frac{\partial f_+}{\partial x} + qE_x\frac{\partial f_+}{\partial p_x} = 0,$$

$$\frac{\partial f_{++}}{\partial t} + \frac{p_x}{m_i}\frac{\partial f_{++}}{\partial x} + 2qE_x\frac{\partial f_{++}}{\partial p_x} = 0,$$

$$\frac{\partial^2\varphi}{\partial x^2} = -\frac{q}{\varepsilon_0}(n_+ + 2n_{++} - n_e),\ E_x = -\frac{\partial\varphi}{\partial x}. \qquad (1)$$

Here, f_e is the electron distribution function (EDF), f_+ and f_{++} are singly-charged and doubly-charged ion distribution functions (IDF), respectively, q is the elementary charge, E_x is the electric field, φ is the electrostatic potential, ε_0 is the vacuum permittivity, m_e and m_i are electron and ion rest masses, respectively. Electron, singly-charged and doubly-charged ion number densities, respectively, n_e, n_+, n_{++} were calculated as zero moments of distribution functions:

$$n_{e,+,++}(x,t) = \int_{-\infty}^{\infty} f_{e,+,++}(x, p_x, t)dp_x.$$

Vacuum diode is series-connected to the voltage source $U(t)$ through the ballast resistance R. At time $t = 0$ the source generates the positive anode potential $U(t)$ with the amplitude U_0 and short rise time ~ 0.1 ns.

In such conditions, solution of the Poisson equation for electric field in plane geometry can be written in the form of exact quadrature expressions

$$E_x(x,t) = -\frac{U(t) - j(t)SR}{D}$$

$$+ \frac{q}{\varepsilon_0 D}\int_0^D\int_0^x \left[n_e(x',t) - n_+(x',t) - 2n_{++}(x',t)\right]dx'dx$$

$$- \frac{q}{\varepsilon_0}\int_0^x \left[n_e(x',t) - n_+(x',t) - 2n_{++}(x',t)\right]dx',$$

$$\varphi(x,t) = \frac{x}{D}(U(t) - j(t)SR)$$

$$- \frac{x}{D}\cdot\frac{q}{\varepsilon_0}\int_0^D\int_0^x \left[n_e(x',t) - n_+(x',t) - 2n_{++}(x',t)\right]dx'dx$$

$$+ \frac{q}{\varepsilon_0}\int_0^x\int_0^{x'} \left[n_e(x'',t) - n_+(x'',t) - 2n_{++}(x'',t)\right]dx''dx'. \qquad (2)$$

Here, $j(t)$ denotes full current density (uniform over the area S) in the power supply circuit with the ballast resistance R. It is defined as a sum of convective current densities of electrons and ions, which are calculated on the basis of the first moments of EDF and IDF

$$j_e(x,t) = q\int_{-\infty}^{\infty}\frac{p_x}{m_e}f_e(x, p_x, t)dp_x,$$

$$j_+(x,t) = q\int_{-\infty}^{\infty}\frac{p_x}{m_i}f_+(x, p_x, t)dp_x,$$

$$j_{++}(x,t) = 2q\int_{-\infty}^{\infty}\frac{p_x}{m_i}f_{++}(x, p_x, t)dp_x$$

and displacement current density, which obeys the full current conservation equation (Ampere's equation)

$$\varepsilon_0\frac{\partial E_x}{\partial t} + j_+ + j_{++} - j_e = j(t).$$

Integration of Ampere's equation with respect to the x coordinate taking into account equation (2) for the field strength $\int_0^D E_x dx = U(t) - j(t)SR$ can give an exact expression for full current density in the circuit

$$j(t) = e^{-Dt/\varepsilon_0 RS}\cdot\int_0^t\left\{\int_0^D (j_+ + j_{++} - j_e)d(x/D)\right.$$

$$\left. - \varepsilon_0\frac{\partial(U/D)}{\partial t'}\right\}\cdot e^{Dt'/\varepsilon_0 RS}d(Dt'/\varepsilon_0 RS). \qquad (3)$$

System of Vlasov–Poisson equations (1) includes initial and boundary conditions describing the injection of cathode plasma through the emission boundary at $x = 0$ (cathode) into the initially empty vacuum gap. Initial distribution functions are assumed to be equilibrium (Maxwellian) with electron temperature T_e and ion temperature T_i:

$$f_{e,+,++}(x, p_x, t = 0),$$

$$f_{e,+,++}(x = 0, p_x, t) = \chi(t)\cdot\frac{n_{0e,+,++}e^{-p_x^2/2m_{e,i}T_{e,i}}}{\sqrt{2\pi m_{e,i}T_{e,i}}}. \qquad (4)$$

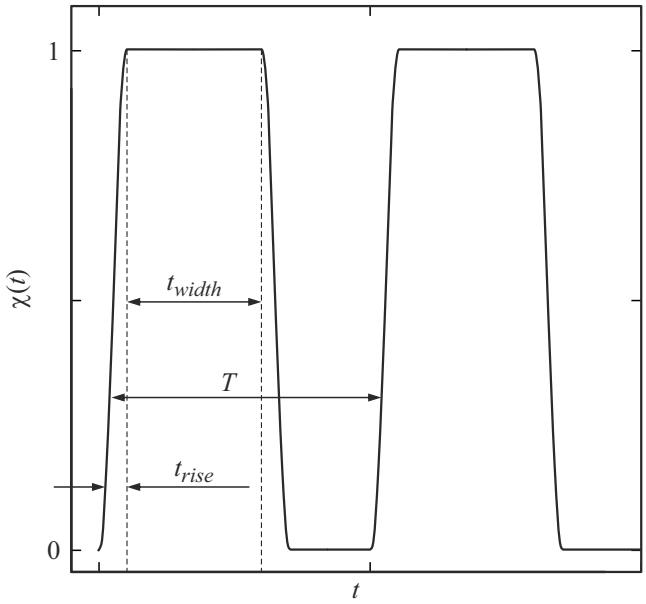

Figure 1. Time dependence of cathode plasma density n_0 in the pulse-periodic mode. T — modulation period, t_{width} — pulse width, t_{rise} — pulse rise time.

Here, $n_{0e} = n_{0+} + 2n_{0++} = n_0$ are determined by the cathode plasma quasi-neutrality condition with a known ion fraction distribution, and $\chi(t)$ is the modulating function of pulse-periodic signal with a arbitrary unit shown in Figure 1.

The study imitates the ecton occurrence and death process using only cyclic boundary conditions (4). Taking into account the known experimental data on single ecton parameters [1–4], the calculations used averaged parameters of $\chi(t)$ shown in Figure 1: $t_{rise} = 0.1$ ns, $t_{width} = 3$ ns, $T = 5$ ns (these are cycle parameters of our „model ecton").

System of Vlasov equations (1) was numerically solved on a quasi uniform grid in phase space variables. Space discretization along the x coordinate is uniformly refined near the cathode in such a way that the size of the smallest element is 10 to 15 times smaller than the characteristic Debye length for the chosen amplitude of the plasma number density n_0 at the cathode. Grid discretization in p_x was assumed to be uniform with boundary values determined by estimated minimum and maximum momentum of plasma particles. Simultaneous solution of three Vlasov equations used a decomposition method (semi-Langrangian numerical scheme), which iteratively decomposes each Vlasov equation into a set of shift equations [20]. Then, a weakly oscillating interpolation method of sufficiently high order of accuracy was used — Steffen's method [21], included in free GNU Scientific Library. Time resolution of the scheme was improved using decomposition methods of the 4th and 6th order of accuracy [22]. Total number of grid elements was 2500 cells in x and 2000 cells in p_x. Mean time step of the numerical scheme was equal to $1-2$ ps.

Results of numerical calculations of the system of equations (1)+(2)+(3) with initial conditions (4) and the following parameters are shown below: Zn cathode, $D = 1$ cm, $S = 1$ cm^2, $R = 200\,\Omega$, $U_0 = 2$ kV, $n_0 = 10^{16}$ cm^{-3}, $n_{0+} = 0.8n_0$, $n_{0++} = 0.2n_0$, $T_e = 5$ eV, $T_{i+} = T_{i++} = 2$ eV.

2. General pattern of current flow and plasma motion

Figure 2 shows the current density time dynamics for current flowing in the vacuum diode, and Figure 3 shows instantaneous density plots of EDF and singly-/doubly-charged IDFs, and longitudinal potential distribution. The current modulation effect is observed throughout the breakdown formation process, i.e. filling the vacuum gap with plasma, starting from the time when the first electrons reach the anode and ending with dense plasma formation to fill the gap completely.

Figure 2 shows that throughout the vacuum breakdown process the total current density in the diode forms a curve with a clearly pronounced modulation frequency. Note that in the cathode emission phase ($\chi(t) = 1$), electron current density has a value approximately by an order of magnitude higher than the Child-Langmuir value $(4\varepsilon_0/9)\sqrt{2q/m} \cdot U_0^{3/2}/D^2 \approx 0.21$ A/cm^2. This was to be expected because dense cathode plasma provides efficient neutralization of the space charge in the virtual cathode cross-section with the maximum density of space charge of electrons. The current density in the diode decreases by only a few times in the intervals between emission cathode phases ($\chi(t) = 0$) because high ion concentration in the cathode region $n_0 = 10^{16}$ cm^{-3} can provide the required conservative current level. And space charge compensation

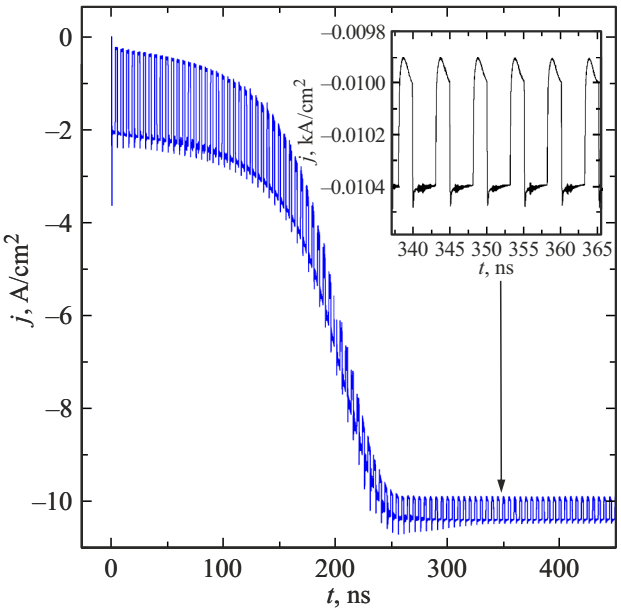

Figure 2. Time profile of full current density of the planar vacuum diode with pulse-periodic emission of quasi neutral plasma from the cathode.

efficiency on the outer (facing the anode) edge of the cathode plasma decreases drastically. As the cathode flare expands, the diode perveance increases monotonically due to a reduction of the length of the „plasma-free“ gap between the flare emission boundary and the anode.

By time 250 ns plasma fills the whole diode gap and current density in the diode is limited by the emission capability of continuously pulsating cathode plasma. Current density modulation amplitude at this stage is not so high any more ($< 5\%$) as at the initial breakdown stage. Reduction of the modulation depth is caused by the fact that at this stage the whole gap is filled with quasi neutral plasma and local space charge effects on the emission capability of a newly emerged ecton are significantly suppressed.

Figure 3 shows cathode plasma motion dynamics in pulsating emission conditions. Distributions are shown for those time points when the cathode emission current reaches its maximum level. In the conditions of interest, the front of the cathode plasma travels to the anode at a superthermal velocity, at which the front of doubly-charged ions Zn^{++} moves. Singly-charged ions, as can be seen, are considerably behind the plasma front movement.

Primary prerequisites for ion acceleration are formed at the edge of the initially quasi neutral cluster (ecton) of the cathode plasma where charge neutrality is violated due to electron density compression in the ecton. In Figure 3 this is indicated by a sharp drop in potential near the cathode cross-section $x = 0$ (right column). Voltage applied to the gap and, accordingly, high electron current on the cathode lead to generation of a negative space charge region where the potential is lower than the cathode potential $\Delta\varphi < 0$ („virtual cathode“). Due to the fact that the external source in the circuit maintains a high anode potential, free electron transport from the outer emission boundary also sets the virtual cathode region in motion, which in turn leads to further ion acceleration under the action of the accelerating electrodynamic force. As a result, the outer plasma emission boundary moves to the anode.

In [17] it is shown that such potential drop and generation of the travelling „virtual cathode“ can provide ion acceleration up to kinetic energies exceeding the depth of potential energy drop $\varepsilon_+ > |q\Delta\varphi|$. Plasma moves in time with the fastest ions (Zn^{++}), starts filling the region between the physical and virtual cathodes and effectively shields the cathode emission region from external voltage.

It is important to emphasize that the cathode plasma expansion mechanism described herein is not associated in any way with collisions between fast electrons and ions, but is of merely electrodynamic origin. Inclusion of the pulsed cathode plasma emission mode into the model or extension to cylindrical and spherical problems don't change the essence of collisionless ion acceleration mechanism.

3. Velocities of ions with different charge numbers within the gap and at the anode

Plasma velocity in the vacuum diode can be experimentally estimated by two methods. Either by directly observing the luminous plasma motion in the gap using high-speed optical survey or by measuring the time required for the vacuum breakdown to switch to the spark phase, for which abrupt increase in the vacuum diode current is typical. Both approaches provide only an estimate of the plasma expansion velocity because all cathode plasma subsystems move at different velocities due to the multi-component nature.

As mentioned above, the moving plasma at the vacuum spark stage is not quasi neutral throughout the interelectrode gap. The cathode has quasi neutral cathode plasma with an electron flow emitted from the outer boundary to the empty space. Cathode plasma expansion takes place at high „superthermal“ velocities, which implies a difference in directed velocities of individual ion components characterized by the magnitude of electric charge. It has been assumed earlier, depending on a hypothesis concerning the physical plasma expansion mechanism, that ions with different charges could move at approximately the same velocities (explosive hypothesis) or at considerably different velocities („potential hump“ hypothesis). From the experimental point of view, there is currently no consensus on this question. For example, Davis and Miller [9] have found that kinetic energy of ions increases approximately proportional to their charge. However, in other studies (for example, experiments [8,13]) measured ion velocities were almost independent of the ion charge number. In all above-mentioned experiments, ion characteristics were measured on the basis of data obtained from ions downstream of the collector (anode).

The calculated mean velocity of the Zn^{++} component can be compared with the experimental velocity measured for the vacuum breakdown of the diode with a pure zinc cathode. Good agreement with the experiment can be seen here. Thus, the experimentally measured mean plasma expansion velocity in the diode with zinc cathode is approx. $2 \cdot 10^6$ cm/s according to [2,3]. In our calculations, the velocity of ion ensemble Zn^{++} can be determined, for example, as an RMS value $\bar{v}_{++} = \sqrt{\int v^2 f_{++} dv / \int f_{++} dv}$. It is important to note that mean velocities of ion components Zn^+ and Zn^{++} significantly exceed the typical values compared with the virtual cathode depth amplitude in terms of kinetic energy $|q\Delta\varphi|$. This is explained by the outer emission boundary motion in a „travelling wave“ type consistent electric field, which is a key feature of the given plasma expansion mechanism. Emission boundary motion and quasi-neutrality violation are very well shown in Figure 4. The cathode plasma emission boundary is positioned where the Zn^{++} and electron concentration curves start diverging. It can be seen that this boundary is determined by the motion of a faster ion component, while

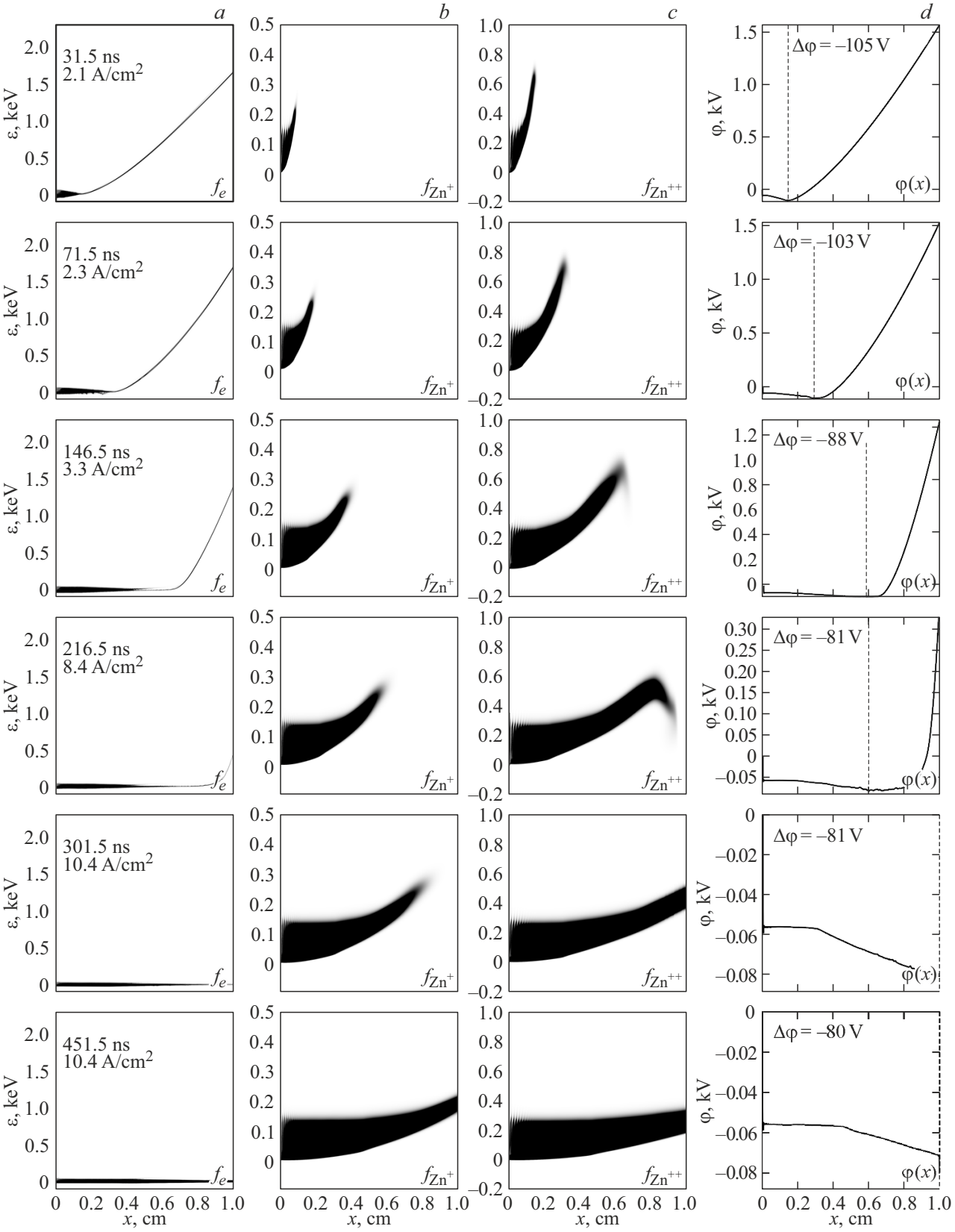

Figure 3. Instantaneous distributions (current time and density are shown in the corner of a column frame): *a* — EDF, *b* — IDF Zn^{+}, *c* — IDF Zn^{++}, *d* — potential. Dashed line on diagrams *d* indicates the potential minimum position (minimum depth is shown in the upper right corner). Gray scale maximum for EDF is normalized to the maximum value at the anode and for all IDF normalized to the same value (10^{38}).

the presence of singly-charged ions Zn^+ doesn't contribute to neutrality violation in any way, though their amount was 4 times larger in the initial plasma.

Simulation results shown in this study support the point of view that the mean ion velocity is directly related to an increase in the ion charge (Figure 3, columns *b* and *c*). But the experiments, where velocities of ions with different charges are approximately equal, can be also explained within our scenario.

Until the plasma fills much of the gap, ion components move with mean kinetic energies, which linearly depend on the charge number, but ions with a higher charge are getting decelerated near the anode. Zn^{++} reach the anode much earlier than Zn^+. In the calculation shown in Figure 3, this occurs approximately at $t = 217$ ns, when the anode potential (multiplied by the charge) is much higher than the kinetic energy of the ion component $\varepsilon_i < qU(t)$. When approaching the anode, the Zn^{++} flux is decelerated at the outer emission boundary of the expanding plasma, while the Zn^+ flux continues its accelerated motion towards the anode in a weak electric field region. This is a critical point of multi-component plasma kinetics!

In our scenario, when the plasma boundary approaches the anode, the anode potential decreases due to charge current growth and to the presence of ballast resistance in the circuit. Ions with all charge numbers reach the anode when moving by inertia because the space between the electrodes is almost equipotential at this time. Velocities of ions with different charges are considerably equalized at the anode (two lower rows: 301 and 451 ns in Figure 3).

Deceleration of the most accelerated (multicharged) components in the experiments probably also leads to equalization of velocities of differently charged ion fluxes when fluxes are recorded downstream of the collector. Variety of experimental results concerning the dependence of mean velocity of multicharged plasma ion components on the charge number doesn't support an experimental error. It likely reflects the effect of various experimental conditions on the measurements. In our calculations, this variety can be simulated by choosing the ballast resistance R in the circuit.

4. Spatiotemporal kinetics of electrons and electric potential in a single cathode plasma emission cycle

Now we explore what's going on during one period of pulsed cathode plasma emission, i.e. one ecton life cycle [23,24]. For this, additional series of calculations was performed with high degree of detail regarding the electron distribution function and potential distribution in the time interval $t = 70-75$ ns covering one cathode emission pulse. To be specific, the 15th ecton cycle in succession from the start of breakdown was chosen. By this time, the virtual cathode (and emission boundary) is located at $x = 0.32$ cm as can be seen in Figure 3 and 4.

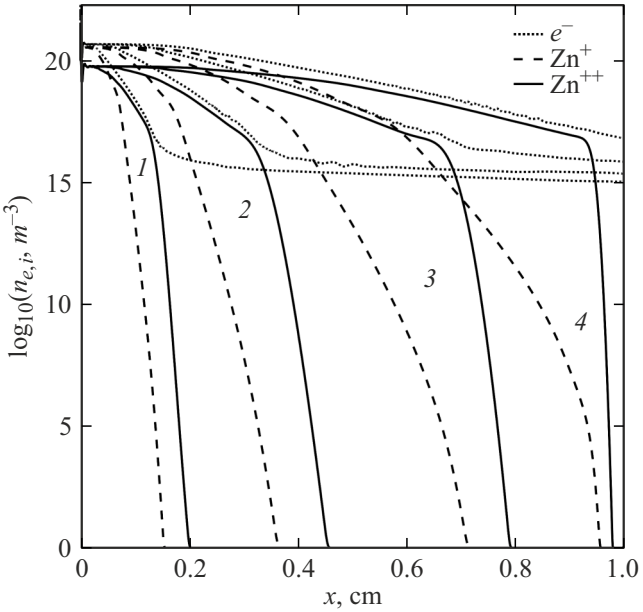

Figure 4. Concentrations of individual expanding plasma components at the following times: *1* — 31.5, *2* — 71.5, *3* — 146.5, *4* — 216.5 ns.

To avoid anode voltage spikes, which hinder this analysis, the calculation was conducted at a fixed anode voltage. Other vacuum diode parameters, cathode plasma composition and density, anode voltage pulse parameters and $\chi(t)$ describing the pulse-periodic cathode emission remained unchanged (Figure 1).

Results of these calculations are shown in Figure 5, which demonstrates instantaneous EDF, IDF and potential distributions in plasma at the cathode for time points marked with numbers in the central time point frame. The frames illustrate what is going on in the gap at each time point of the modulated ecton emission starting from $t = 70$ ns, when the emission was switched off during approx. 2 ns after the previous cycle (phase portrait *1* in Figure 5). Starting from $t = 70.1$ ns, when the emission current jumps up to the maximum value (ecton plasma starts flowing into the vacuum gap), and the potential distribution profile undergoes significant changes before the end of the emission phase at $t = 73$ ns. In the neighborhood of the plasma emission boundary, the virtual cathode with amplitude $\Delta\varphi = -100$ V is formed (as in Figure 3) and demonstrates all previously described typical features: abrupt potential drop of about -50 V near the cathode and a more gently sloping potential curve length leading to a point of minimum $\Delta\varphi = -100$ V. Within this time interval, there is injection of electrons (phase portraits *2–3–4* in Figure 5) induced by generation of another ecton. In the plasma emission interval (between active phases of successive ectons), EDF also has dramatic features (phase portraits *5–6* in Figure 5). During the ecton lifetime $t_{width} = 3$ ns, there is a small plasma transfer caused both by an electric field and by inertial properties of an ion

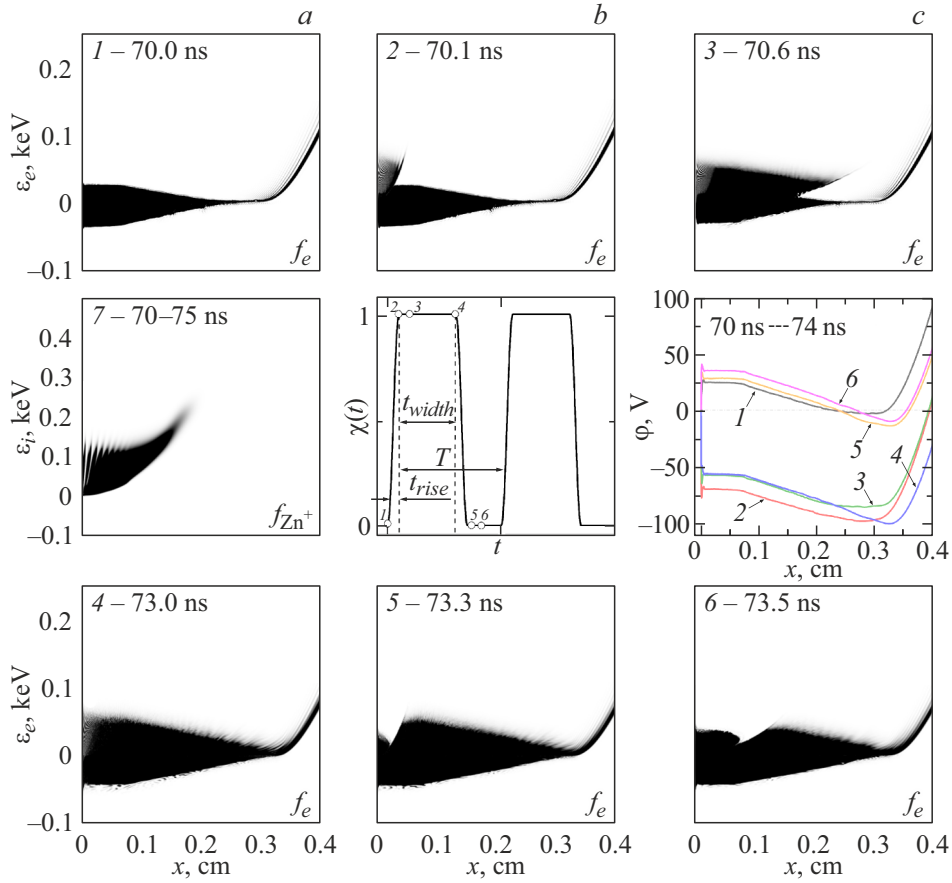

Figure 5. EDF and IDF phase portraits, and electric potential distributions near the cathode in different times of one full plasma emission cycle: 70−75 ns. EDF portraits *1*−*6* and potential curves refer to time points shown on the $\chi(t)$ curve (frame in the center). IDF of the full cycle is shown in portrait *7*. Density of shades of gray is normalized to the same value (10^{40}).

component. This cyclic transfer is clearly seen in the IDF portrait (phase portrait *7* in Figure 5).

Compared with a continuous cathode plasma emission described in [14,15], pulse-periodic mode leads to global potential oscillations in the gap between the cathode and outer plasma boundary. Potential distributions in the middle right frame in Figure 5 demonstrate important features. In the interval between emission pulses (time points *1, 5, 6* in the central frame in Figure 5) corresponding to active functioning of ectons, potential distribution has a typical „potential hump" form. When emission is resumed, „virtual cathode" distribution is generated throughout its length (time points *2*−*4* in the central frame in Figure 5) regardless of the distance between the outer plasma boundary and the cathode. Ecton death leads to „throw-up" of the potential on the plasma, and appearance of a new ecton restores the virtual cathode with its original amplitude $\Delta\varphi$. Comparison of lines *4* and *5* indicates that it is exactly the „throw-up" (during the time shorter than 1 ns) of the existing space structure: they are almost identical. The cathode plasma after ecton extinction is actually charged as a whole approximately by +100 V. Maintenance of the space structure of the electric field provides continuous action of the field-induced plasma expansion mechanism despite the pulsed ecton plasma emission mode. During this process, anode voltage remains constant (2 kV) and virtual cathode depth modulation within $\Delta\varphi = \pm 100$ V changes the voltage applied to the „plasma-free space of the vacuum diode. Modulation of the applied voltage leads to oscillations of the electron beam current (or vacuum spark current) even at the switching stage, as shown in Figure 2.

Short delay time before generation of a new ecton has no significant effect on IDF. This is associated with the fact that ions, being heavier than electrons, move in this time interval to the anode due to their inertia. Nevertheless, space charge fluctuations in the vacuum diode cause some changes in IDF. Figure 5 shows the IDF distribution in the interval $t = 70-75$ ns, where a typical serrated structure of IDF near the cathode can be seen. This feature is induced by multiple fast potential redistributions in pulse-periodic emission mode. It is completely absent in calculations where the cathode emission is assumed to be continuous, for example, in [14,15].

Another effect that should be noted is considerable heating of electron gas in the cathode plasma, which is caused by potential oscillations in the initial cross-section

($x = 0$). This is directly indicated by electron phase portraits in Figure 5. This is the same mechanism, which is responsible for ion acceleration to „superthermal“ velocities as shown in [17].

Discussion and conclusions

The above-mentioned results of kinetic simulation of the vacuum discharge can be treated as a baseline spark stage scenario because it correctly reflects all observed properties both in terms of quality and quantity.

1. Appearance of dense plasma on the cathode initiates the fundamental electrodynamic plasma expansion mechanism, which drives ion acceleration to „superthermal“ velocities at a level of $(2-5) \cdot 10^6$ cm/s. The main structure in this mechanism is the „virtual cathode“–„potential hump“ electric field distribution in an alternating manner depending on the „active ecton“–“ emission pause“ cathode emission phases, respectively (Figure 5).

In this light, the hypothesis for a „potential hump“ in a vacuum discharge first suggested by Plyutto [5] appeared to be true. And there is a reference to a deep potential well in the neighborhood of the vacuum discharge plasma cathode, which can be interpreted as a „virtual cathode“, in the work by Barengolts et al [25].

2. Electric field mechanism in the initial vacuum spark phase provides higher velocities of ions with higher charge number than those of ions with lower charge number. But at the end of the spark phase, when plasma approaches the anode, the discharge switches to the arc phase with low anode voltage, ions with high charge number are considerably decelerated. Slower ions moving by inertia in already weakened field reach the anode at velocities, which are not much different from velocities of faster ions (Figure 3). Here, depending on the circuit parameters, there may be different situations, which can explain the known spread of experimental data on velocities of ions with different charge numbers obtained by different research teams [5–7,9,11–13].

Vacuum spark calculations in the spherical $1D$ geometry taking into account collisions by the PIC–MCC method (Particle-in-Cell & Monte Carlo Collision) have been described recently in [26] and have confirmed that there was the proposed field-induced mechanism of ion acceleration up to high velocities. But particle collisions, according to the PIC–MCC calculations, lead to considerable equalization of velocities of ions with different charge numbers in a wide „potential valley“ (synonym of the „virtual cathode“).

3. Kinetic calculations of electrophysical properties of the vacuum diode with plasma cathode provide correct estimate of the diode perveance and electron beam generation phase time (Figure 2). Perveance of the diode with plasma cathode in active phase is approximately by an order of magnitude higher than the Child–Langmuir perveance $P_{\mathrm{CL}} - (4\varepsilon_0/9)\sqrt{2q/m}/D^2$ because the space charge of electrons at the emission boundary is considerably compensated. Calculated time of electron beam generation in the diode ($D = 1$ cm) of ~ 150 ns (Figure. 2) is in good agreement with the experimental data.

Of course, it would be too arrogant to believe that a simplified one-dimensional collisionless model of the phenomenon could explain all behaviors observed in the vacuum discharge. We only suggest that even idealized setting of the problem allowing mathematically accurate quantitative solution gives correct estimates for key vacuum discharge parameters. This suggests a fundamental phenomenon mechanism, which acquires additional details and aspects in different particular cases.

Funding

The work was carried out under the state assignment of the Ministry of Science and Higher Education of the Russian Federation on topics № FWRM-2021-0007, FWRM-2021-0014.

Conflict of interest

The authors declare no conflict of interest.

References

[1] G.A. Mesyats, *Ektony v vakuumnom razryade: proboi, iskra, duga* (Nauka, M., 2000) (in Russian).
[2] R.L. Boxman, D.M. Sanders, P.J.T. Martin. *Handbook of vacuum arc science and technology: fundamentals and applications* (Noyes Publications, New Jersey, 1995)
[3] A. Anders. *Cathodic Arcs: From Fractal Spots to Energetic Condensation* (Springer, NY., 2008), DOI: 10.1007/978-0-387-79108-1
[4] *Vacuum arcs: theory and application*, ed. by J.M. Lafferty (Wiley, NY., 1980)
[5] A.A. Plyutto, V.N. Ryzhkov, A.T. Kapin. ZhETF, **47** (8), 494 (1964) (in Russian).
[6] E.D. Korop, A.A. Plyutto. ZhTF, **40** (12), 2534 (1970) (in Russian).
[7] E.D. Korop, A.A. Plyutto. ZhTF, **41** (5), 1055 (1971) (in Russian).
[8] E.M. Oks, K.P. Savkin, G.Y. Yushkov, A.G. Nikolaev, A. Anders, I.G. Brown. Rev. Sci. Instrum., **77** (3), 03B504 (2006). DOI: 10.1063/1.2164967
[9] W.D. Davis, H.C. Miller. J. Appl. Phys., **40** (5), 2212 (1969). DOI: 10.1063/1.1657960
[10] I.A. Krinberg. ZhTF, **71** (11), 25 (2001) (in Russian).
[11] V.I. Krasov, V.L. Paperny. Fizika plazmy, **43**, 3 (241) (in Russian). (2017). DOI: 10.7868/S0367292117030076
[12] A. Anders. In: *Proceedings of 2014 International Symposium on Discharges and Electrical Insulation in Vacuum* (*ISDEIV*) (IEEE, Mumbai, 2014), p. 201. DOI: 10.1109/DEIV.2014.6961796
[13] G.Yu. Yushkov, A.S. Bugaev, I.A. Krinberg, E.M. Oks. DAN, **46** (5), 41 (2001).
[14] V. Kozhevnikov, A. Kozyrev, A. Kokovin, N. Semeniuk. Energies, **14** (22), 7608 (2021). DOI: 10.3390/en14227608

[15] A.V. Kozyrev, V.Yu. Kozhevnikov, N.S. Semeniuk, A.O. Kokovin. Plasma Sourc. Sci. Technol., **32** (10), 105010 (2023). DOI: 10.1088/1361-6595/acfff1
[16] V.Yu. Kozhevnikov, A.V. Kozyrev, A.O. Kokovin, N.S. Semenyuk. Fizika Plazmy, **49** (11), 1170 (2023) (in Russian). DOI: 10.31857/S036729212360060
[17] V.Yu. Kozhevnikov, A.V. Kozyrev, V.S. Igumnov, N.S. Semenyuk, A.O. Kokovin. Izv. RAN. MZhG, **6**, 183 (2023) (in Russian). DOI: 10.31857/S1024708423600446
[18] A.V. Kozyrev, V.Yu. Kozhevnikov, A.O. Kokovin. Pisma v ZhTF (in Russian), **50** (22), 25 (2024). DOI: 10.61011/PJTF.2024.22.59131.20022
[19] A. Anders. Phys. Rev. E, **55** (1), 969 (1997). DOI: 10.1103/PhysRevE.55.969
[20] G. Strang. SIAM J. Numer. Anal., **5** (3), 506 (1968). DOI: 10.1137/0705041
[21] M. Steffen. Astron. Astrophys., **239**, 443 (1990).
[22] H. Yoshida. Phys. Lett. A, **150** (5–7), 262 (1990). DOI: 10.1016/0375-9601(90)90092-3
[23] G.A. Mesyats. UFN, **165** (6), 601 (1995) (in Russian). DOI: 10.3367/UFNr.0165.199506a.0601
[24] H.T.C. Kaufmann, C. Silva, M.S. Benilov. Plasma Phys. Controlled Fusion, **61** (9), 095001 (2019). DOI: 10.1088/1361-6587/ab2fac
[25] S.A. Barengolts, N.Yu. Kazarinov, G.A. Mesyats, E.A. Perelshtein, V.F. Shevtsov. Pis'ma v ZhTF, **31** (4), 64 (2005) (in Russian).
[26] M. Song, H. Zhang, Q. Sun, W. Yang, Z. Wang, Z. Liu, Y. Dong, Q. Zhou. Plasma Sourc. Sci. Technol., **33** (10), 105009 (2024). DOI: 10.1088/1361-6595/ad7c7a

Translated by E.Ilyinskaya